# Genetically Engineering Exciton Networks in Light-Harvesting Antennas to Enhance Energy Transport

Heechul Park,[1,2†] Nimrod Heldman,[1,2†] Patrick Rebentrost,[3] Luigi Abbondanza,[4] Alessandro Iagatti,[5] Andrea Alessi,[4] Barbara Patrizi,[5] Mario Salvalaggio,[4] Laura Bussotti,[5] Masoud Mohseni,[3] Filippo Caruso,[5,6] Hannah C. Johnsen,[7] Roberto Fusco,[4] Paolo Foggi,[5,8,9] Petra F. Scudo,[4*] Seth Lloyd,[3,10*] and Angela M. Belcher[1,2,7*]

[1]Department of Materials Science and Engineering, Massachusetts Institute of Technology, Cambridge, Massachusetts 02139, USA
[2]The David H. Koch Institute for Integrative Cancer Research, Massachusetts Institute of Technology, Cambridge, Massachusetts 02139, USA
[3]Research Laboratory of Electronics, Massachusetts Institute of Technology, Cambridge, Massachusetts 02139, USA
[4]Research Center for Non-Conventional Energy, Istituto ENI Donegani, ENI S.p.A., Novara 28100, Italy
[5]European Laboratory for Non-linear Spectroscopy, University of Florence, Sesto Fiorentino 50019, Italy
[6]QSTAR and Department of Physics and Astronomy, University of Florence, Florence 50125, Italy
[7]Department of Biological Engineering, Massachusetts Institute of Technology, Cambridge, Massachusetts 02139, USA
[8]Department of Chemistry, University of Perugia, Perugia 06123, Italy,
[9]INO CNR, Sesto Fiorentino 50019, Italy
[10]Department of Mechanical Engineering, Massachusetts Institute of Technology, Cambridge, Massachusetts 02139, USA

[†]These authors contributed equally to this work.

*Corresponding authors. E-mail: petra.scudo@eni.com, slloyd@mit.edu, belcher@mit.edu

**Abstract**

**Efficient exciton transport in light-harvesting systems is of essence for designing solar energy technologies. One of the challenges for achieving such efficient transport is precise structural control of the light-harvesting building blocks. Here,**

**we create a tunable material consisting of a 3D chromophore network on an ordered biological virus template. This system establishes a genetic link between the chromophores and their emerging transport properties. The combination of spectroscopy measurements and dynamic modeling enables us to illuminate the interplay of quantum coherent and classical, incoherent energy transport at room temperature. Through genetic modifications, we obtain a significant enhancement of the energy transport in an intermediate quantum-classical regime.**

A diverse range of materials has been investigated for efficient exciton transport and solar energy conversion applications. Some of the challenges are precisely controlling structures on the level of individual light-harvesting building blocks and understanding the role of the interplay of coherent and incoherent dynamics. For most organic light-harvesting materials, such as cyclic dye systems, dendritic structures, and J-aggregate nanotubes [1-3], chromophore selection, the structural arrangement of chromophores, and inter-chromophoric couplings play a crucial role in their design, as also shown in natural light-harvesting [4,5]. In addition, quantum transport in contrast to a semi-classical hopping mechanism has been suggested to contribute to high efficiency in such natural systems [6-9]. Biological materials including DNA and tobacco mosaic viruses can serve as templates for light-harvesting assemblies [10-12]. The M13 virus has been shown to be a versatile and tunable engineering tool with a large range of applications such as batteries, solar cells, water splitting, and cancer imaging [13-16]. The M13 virus has chemically reactive conjugation sites, which allows assembling diverse types of chromophores. In previous work, we have shown that the wild type M13 virus can be

used for building a light-harvesting assembly of zinc porphyrins, and proposed that Förster resonance energy transfer (FRET) and Dexter mechanism are involved in the transport process [17].

Here, we create a light-harvesting antenna system that shows genetically enhanced exciton transport. We demonstrate that the M13 virus can act as a tunable chromophore scaffold carrying donors and acceptors and explore the underlying mechanism of the efficient transfer of energy in this light-harvesting antenna system. The use of programmable genes allows us to manipulate the positioning of the binding sites and thus multiplies the possibilities for creating intricate chromophore networks and for controlling the energy transfer. Two types of M13 viruses are genetically engineered: one virus is shown to have a regular network of weakly coupled chromophores, and the other is engineered to have clusters of strongly coupled chromophores. By a combination of room temperature spectroscopy experiments and theoretical models for the exciton dynamics based on resonant coupling and delocalization, we demonstrate that the weakly coupled network exhibits slow semi-classical Förster energy transfer and that the genetically improved strongly coupled network resides in a regime where coherent and incoherent transport collaborate for boosting exciton diffusion. So far, the enhancement of energy transport due to interplay between coherent and incoherent dynamics has been shown only theoretically [9,18]. Here, we provide the first experimental evidence for such an enhancement in a designed system. The genetically improved antenna achieves a longer diffusion length by 68% over the other antenna and a four-fold increase in the number of donors contributing energy to a single acceptor.

The two types of M13 viruses were engineered by modifying the amino acid sequence of the pVIII protein, which serves as a building block for the chromophore network (Fig. 1). The virus consists of a highly ordered filamentous array of 2,700 copies of the pVIII proteins. We name the two clones M13CF (CF for Classical Förster) and M13SF (SF for Super-Förster). We used previously obtained structural data (Protein Data Bank (PDB) number 2C0W) to reconstruct the model of both clones in order to estimate the distances between chromophore binding sites [19]. The primary amine groups of the pVIII exposed on the surface, N-terminus and lysine residues, can act as specific binding sites for chromophores. The M13CF virus bearing the amino acid sequence of ADSPHTELPDPAK at the N-terminal region of the pVIII [14] was used because the distances between the two primary amines are longer than the corresponding distances in the wild type. The inter-binding site distance was estimated to be 33 Å on the pVIII (Fig. 1c). In order to create an entirely different network with closer distances, the M13SF virus was genetically engineered to have an additional third binding site on the pVIII. Among the possible candidates (data not shown), the M13SF carrying the shorter pVIII N-terminal sequence of AENKVEDPAK was identified as having inter-binding site distances of 10 Å on the pVIII (Fig. 1b). These distances are short enough to enhance the coupling strength of the bound chromophores, but long enough to avoid the complete quenching of fluorescence due to short-range Dexter exchange [5,20]. The electronic coupling strength between donors for the 10 Å distance is about 460 $cm^{-1}$, calculated using the standard FRET exchange formula and the spectral overlap, and assuming parallel orientation of the dipoles, see supporting information.

Various kinds of chromophores can be selected for coupling to the M13 virus biological scaffold through chemical modification of amine groups on the pVIII coat proteins. Zinc porphyrins were used at the beginning of this work, but experimental and theoretical results showed that the electronic couplings between the porphyrins are too weak for our purposes. Alexa Fluor® 488 and Alexa Fluor® 594 were carefully selected as donor and acceptor chromophore, respectively (Supplementary Fig. 1). They show narrow and well-separated absorption bands and good spectral overlaps between donor emission and donor absorption as well as between donor emission and acceptor absorption for energy transfer (Fig. 2a). Absorption peaks are at 491 nm for the donor and at 585 nm for the acceptor. Emission peaks are at 517 nm for the donor and at 611 nm for the acceptor. The acceptor emission peak is sufficiently far from the donor emission peak to resolve the signals of fluorescence when the donors are excited and the fluorescence intensities are detected from the acceptors. They also show high molar extinction coefficients (i.e. strong transition moments) and relatively high quantum yields [21]. Both donors and acceptors have additional advantages such as good water solubility, photo-stability, and pH insensitivity [22]. They also have no tendency to aggregate because of a net negative charge and steric hindrance [23]. Moreover, a pre-activated carboxylic acid in each donor and acceptor allows for specific conjugation to the primary amines on the pVIII by forming covalent amide bonds. These properties render the chromophores good candidates for creating energy transport networks on the M13 virus.

A dense occupation of the sites comprising the energy transfer network on the M13 virus surface is desired. The experiments were conducted at pH 7.4 where the percentage of reactive sites was estimated to be about 39% for the N-terminus and 1% for

the lysine (see Supplementary Information). By this estimation, conjugation to the N-terminus is more probable than to the lysine. In order to overcome the low probability of labeling the lysine, 20-fold excess of chromophores over the pVIII binding sites were added. The samples were then extensively purified to remove unreacted chromophores completely. The chromophore conjugation along the virus was observed by fluorescence microscopy (Fig. 2b upper inset) and attachment to the pVIII was confirmed by both polyacrylamide gel electrophoresis and mass spectroscopy (see Supplementary Information). The numbers of chromophores on the M13 virus were calculated from the measured absorbance. An average of 4,130 ± 70 donors on the M13SF were assembled among the total possible binding-sites of 8,100 per virus, while 2,970 ± 180 donors on the M13CF were assembled among 5,400 total sites. Knowing the probability of amine labeling on the M13CF virus, it was estimated that 2,700 N-termini are fully occupied with the chromophores (~ 100%) and only ~ 200 lysine residues are occupied (~ 7%). Similarly, in the M13SF it was estimated that all 2,700 N-termini are fully labeled (~ 100%), ~ 200 on the pre-existing lysine residues (~ 7%), and ~ 1,200 on the newly added lysines (~ 44%). The higher probability of the new lysines to be labeled may result from a lower $pK_a$ value arising from two glutamic acids located near it [24]. As a result, there are around 1,200 out of 2,700 pVIII copies with 10 Å inter-chromophore distances.

The symmetrically ordered assembly of the pVIII forming the M13 virus is the foundation for the chromophore networks (Fig. 1b,c). The two different grids are determined by the genetic design of the pVIII and the occupation probabilities of the binding sites as given above. The M13CF is closer to an ideal diamond grid of relatively well-separated N-terminus chromophores (Fig. 1c). Because the semi-classical Förster

rates of transport depend on the distance r as $1/r^6$ [20], we can assume that each chromophore has four relevant nearest neighbors. The M13SF has the same basic diamond grid but about 50% of the unit cells have additional vertices resulting from the lysines, which fill the empty space (Fig. 1b). The distance between nearest neighbors resides within the Förster radius between donors, which is estimated to be 37.5 Å on the M13CF, and 30 Å on the M13SF (see Supplementary Information). This guarantees connectivity of the network with at least more than 50% inter-chromophoric energy transport on both clones. For the M13SF, we expect that the stronger electronic couplings and the subsequent highly linked network lead to improved energy transport.

There exists an optimal distance between chromophores where the strong couplings lead to fast transport, but the increased exciton loss from concentration quenching does not dominate. The quenching of donor fluorescence is observed in both clones at a constant donor absorbance of 0.3 with 1 cm path length in order to minimize the inner filter effects of the donors. M13SF shows more quenching than M13CF, which in turn shows more quenching than the free donors (Fig. 2b). Quantum yields for the samples were 1% for the M13SF and 5% for the M13CF, compared to a value of 92% for free donors. This quenching can be explained by the close proximity between chromophores. In order to test this explanation, a control sample of more sparse chromophores, ~400 donors on the M13SF, was prepared. This sample showed significantly less quenching than both previous samples (Fig. 2b), suggesting that the quenching effect comes largely from the inter-chromophoric interactions, rather than from the protein conjugation.

Acceptor chromophores were scattered within the donor grid on the M13 virus to act as output sensors of exciton diffusion. When the donors on the M13 virus are excited, the excitation energy transfers between the donors until it reaches an acceptor. Once the acceptor receives the energy, then a part of the transferred energy is detected from the acceptors in the form of fluorescence intensities. In order to obtain quantitative insights into the exciton diffusion and the maximum number of donors contributing to a single acceptor, different ratios of the donors to acceptors were assembled along the viruses. Constant concentrations of donors with a varied concentration of acceptors were mixed into the solution of the virus. The total number of chromophores on the virus remained approximately constant (4,110 ± 250 for M13SF and 2,920 ± 240 for M13CF), while the number of acceptors bound to the virus surface varied. The samples had donor to acceptor ratios from 16:1 to 734:1 for M13SF and the ratios from 19:1 to 394:1 for M13CF. The ratios were estimated by absorbance. The donor absorbance shows peak shifts to 497 nm for the M13SF and 496 nm for the M13CF, which is evidence of an electronic coupling of the chromophores (Supplementary Fig. 6). All the samples were adjusted to the same donor absorbance at 495 nm at a level high enough to detect the fluorescence signal of the acceptors (Supplementary Fig. 3 and 4).

Steady-state fluorescence of the acceptors shows their sensitization by the donors. In the room temperature measurements of steady-state fluorescence, all samples of the light-harvesting nanoantennae were excited at 495 nm, so that they absorb the same maximum number of incident photons. The emission near 610 nm is essentially ascribable to the acceptor as a consequence of energy transfer from the donor chromophores, while the 520 nm band is due to the donor emission. The overlapping

background fluorescence of the donors was subtracted from the acceptor emission signal. Each spectrum of fluorescence was integrated over wavelength to obtain the total energy of fluorescence emitted from the acceptors (Fig. 3a). With increasing acceptor concentration the total fluorescence increases at first and saturates for large acceptor concentrations. The saturation can be explained by a competition of the acceptors for the available excitation energy from the donors.

The fluorescence data also enable us to elucidate the number of donors contributing to a single acceptor as well as the excitonic diffusion length. The integrated fluorescence was normalized by the number of acceptors to obtain the total energy emitted from a single acceptor as a function of the donor to acceptor ratio (Fig. 3b). Maximum fluorescence energy per acceptor for the M13SF was at a donor to acceptor ratio of 432:1 and for the M13CF at a ratio of 98:1. We developed a phenomenological fitting method to extract a quantitative estimate of exciton diffusion length (Fig. 3b). The fitting function is based on the rationale that each acceptor harvests energy from a given area of donors on the virus. The acceptors compete for the available total area on the virus and, as their concentration increases, the harvesting areas of the acceptors overlap which reduces the single acceptor trapping probability as exhibited by the saturation in Fig. 3a (see details in Supplementary Information). The diffusion length is defined to be simply the radius of the harvested area around an acceptor and is obtained by the fitting to be 7.8 nm for M13CF, and 13.1 nm for M13SF, demonstrating an improvement of ~ 68%. With the same theory, the number of donors contributing to the fluorescence of a single acceptor was estimated to be 29 for M13CF and 114 for M13SF, a four-fold increase. In contrast, one can obtain an estimate of the exciton diffusion length solely

from the Förster radius and the average chromophoric distance using a simple random walk model for excitons, which results in 5.8 nm for M13CF and 6.6 nm for M13SF (see Supplementary Information). The experimental data show a significant improvement of energy transfer in M13SF relative to M13CF, which is not predicted by Förster theory.

Room temperature measurements of transient absorption (TA) spectroscopy reveal further experimental details about exciton dynamics. These measurements show that the excited state decay rate of the donor is twice as fast in the densely clustered M13SF clone than in the M13CF clone. The samples were pumped with a 100 fs laser [25] off the donor absorption peak, at 470 nm, in order to clearly see the wavelength range of bleaching at 500 nm. They were probed over a wide wavelength range from 350 nm to 650 nm. Figure 4a shows the time dependent behavior of the optical density change across the measured spectrum for the M13SF with ~ 4,100 donors. The normalized bleaching spectra show distinctive differences of excitonic behavior between the donors on the M13 virus samples and free donors in the decaying component (Fig. 4b). The bleaching spectra were fitted by a triple-exponential decay function and the resulting lifetimes were averaged (see details in Supplementary Information). It was estimated from the laser intensity that 10% of the chromophores are excited at once, which implies a contribution of singlet-singlet annihilation to the TA signal. This contribution was estimated to occur mainly on short times scales and hence does not substantially affect the estimated averaged exciton lifetimes (see Supplementary Information). The averaged excited state lifetime of both clones was dramatically reduced compared to the lifetime of 4.1 ns for donors free in solution. The averaged lifetime of the M13SF antenna with ~ 4,100 donors was measured to be 90 ps, about ~ 2 times faster than the M13CF with ~

2,900 donors and a lifetime of 184 ps. The sample with ~ 400 donors on the M13SF exhibited a decay time of ~ 2 ns, similar to free donors: the differences can be explained largely by chromophore-protein interactions. The presence of acceptors reduced the donor excited state lifetimes (Supplementary Table 3), because of additional donor-to-acceptor transfer processes. The data for the M13SF with ~ 4,100 donors are plotted in the inverse of the lifetime (i.e. the rate constant) as a function of the acceptor-to-donor ratio (Supplementary Fig. 15). By measuring donor bleaching, a similar trend emerges to the trend of the Fig. 3a: the more acceptors, the faster the donor excited state decay rate. The shorter excitation energy lifetime in the M13SF antenna of about 90 ps arises from the strong interactions between chromophores located close to each other.

In order to obtain more detailed insight into the exciton dynamics, we set up a numerical simulation to predict our experimental results using three theories: a classical walk (CW), a decohered quantum walk (DQW) and a phenomenological Super-Förster theory (SFT). A classical walk describes the exciton motion as hopping between sites. The decohered quantum walk and the Super-Förster theory allow for strong inter-chromophore couplings and quantum coherence effects. We take into account the estimated detailed structural information, distance and network connectivity, and the probabilities of chromophore occupation at each binding site. Studying ensembles of virus-chromophores complexes enables us to only require knowledge of the averaged site occupation and also the averaged orientation of the chromophores. The Förster couplings are derived from the Förster radii and the spectral overlap. The averaged relative dipole orientation is taken as the only free parameter, giving good results for a value reasonable for a non-isotropic averaged system, see Supplementary Information. As a result, the CW

numerical simulation predicted the fluorescence data of the M13CF while it underestimated the performance of the M13SF (Supplementary Fig. 21 and 22). For the M13SF, we employed a decohered quantum walk model. It is based on a tight-binding Hamiltonian with the Haken-Strobl-Reinecker noise model [26,27] and with estimates for the amount of site-energy static disorder and the dephasing rate. While the model describes an infinite temperature pure-dephasing approximation, it includes exciton delocalization and strong coupling effects leading to clustering and allows us to simulate relatively large networks. It predicts the fluorescence data for the M13SF virus well (Fig. 5). Comparing the two theories confirms that the exciton transfer of M13CF is well described by semi-classical Förster theory while the clustered network of the M13SF clone warrants a more careful treatment that takes into account strong couplings and quantum delocalization over clusters of donors.

In addition, we developed the SFT in order to untangle the clustering effects of dipole moment and chromophore distance contained in the DQW model. It is based on the rationale that due to random disorder and strongly coupled dipole moments, in the transfer process excitons are delocalized on clusters of a few chromophores, while performing a classical hopping between adjacent clusters. First, these clusters can be considered as super-molecules sharing a collective transition dipole moment. Second, the spatial extent of the clusters in the M13SF reduces the effective distances between the clusters compared to the almost regular diamond grid of the M13CF. To get an idea of the clustering in the M13SF, the occupation probabilities of the binding sites predict that about 1.43 chromophores participate in a cluster on average, see Supplementary Information. With these two Super-Förster corrections, we can simulate the exciton

propagation among such clusters, for a wide range of acceptor concentrations. As a result, the SFT prediction follows the fluorescence data of M13SF reasonably well, with the distance correction being the dominating effect.

The various data support stronger inter-chromophoric electronic coupling in the M13SF. Upon assembly of the chromophores, the absorbance peaks shift to the red, and significant fluorescence quenching is observed. The enhanced diffusion length, transient absorption measurements, and excitonic dynamics simulations also suggest that our system has strong couplings, and that semi-classical Förster theory, valid only in the assumption of weak electronic coupling, cannot be applied. Both stronger couplings and excitonic delocalization play a key role in boosting excitation energy transfer in the M13SF light-harvesting antenna.

In this work, we have created a tunable light-harvesting material by using a genetically modifiable, self-assembled virus template. It enables us to sample chromophore network configurations along the spectrum between coherent and incoherent exciton transport. We have created an intermediate configuration showing improved exciton transport compared to an incoherent transport configuration. This improvement arises beyond a regime of semi-classical Förster transport from a stronger coupling between the chromophores, where usually quantum coherence effects accompany the enhancement of transfer. We thus exhibit an important design concept previously discussed only theoretically: quantum coherence and incoherent mechanisms can interplay to enhance exciton transfer. This design concept is robust with respect to variation of specific implementation details, such as vibrational environment or loss pathways. Our system may prove especially useful for investigating such higher-level

energy transport mechanisms, for example exciton relaxation effects and directing the exciton transport towards specific sites. In addition, we lay the fundamentals for a wide range of applications relying on efficient energy transfer, such as organic photovoltaics, and light-driven catalysis.


## Acknowledgements

This work was supported from Eni, S.p.A. (Italy) through the MIT Energy Initiative Program. H.P. thanks Kwanjeong Educational Foundation for its financial support, and Dr. Gyu Weon Hwang for allowing us to use a fluorometer. F.C. has been supported by EU FP7 Marie-Curie Programme (Career Integration Grant) and by MIUR-FIRB grant (Project No. RBFR10M3SB).


## Author contributions

H.P., N.H., P.F.S., M.M., R.F., S.L., and A.M.B. conceived the work. P.F.S., P.F., S.L., A.M.B. supervised the overall work. H.P., N.H. designed the experiments including protocols. H.P. prepared all the samples, performed the spectroscopic measurements, analyzed the data and interpreted the data with classical Förster theory. H.P. wrote a first version of the manuscript, based on which H.P., N.H., P.R. developed the final version of the manuscript. H.P., N.H. reconstructed the virus structure models, and performed the virus cloning. P.F.S., R.F. made collaborations between MIT and Italy. P.R., P.F.S., L.A., M.M., R.F. and S.L. designed the theoretical work. P.R., M.M., S.L. developed the fluorescence theory, and P.R., H.P. applied it to the data. P.R., S.L. developed the quantum transport theory, and P.R., L.A. performed the quantum mechanical simulations.

A.I., B.P., L.B., P.F. performed the TA measurements, and analyzed the TA data. P.F., H.P. interpreted the TA data. M.S., R.F. helped H.P., N.H., A.A. perform the QY measurements, and H.P., A.A. analyzed the QY data. F.C. collaborated in developing the computation model. H.C.J. helped H.P. for the virus preparations. H.P., N.H., P.R., P.F.S., S.L., and A.M.B. made major edits on the manuscript. All the authors gave helpful comments on the manuscript.

## Competing financial interests

The authors declare no competing financial interests.

## References


1. Wasielewski, M. R. Self-Assembly Strategies for Integrating Light Harvesting and Charge Separation in Artificial Photosynthetic Systems. *Accounts of Chemical Research* **42**, 1910-1921 (2009).
2. Goodson, T. G. Optical excitations in organic dendrimers investigated by time-resolved and nonlinear optical spectroscopy. *Accounts of Chemical Research* **38**, 99-107 (2005).
3. Eisele, D. M. *et al.* Utilizing redox-chemistry to elucidate the nature of exciton transitions in supramolecular dye nanotubes. *Nature Chemistry* **4**, 655-662 (2012).
4. Blankenship, R. E. *Molecular mechanisms of photosynthesis*. (Blackwell Science, 2002).
5. Scholes, G. D., Fleming, G. R., Olaya-Castro, A.&van Grondelle, R. Lessons from nature about solar light harvesting. *Nature Chemistry* **3**, 763-774 (2011).
6. Engel, G. S. *et al.* Evidence for wavelike energy transfer through quantum coherence in photosynthetic systems. *Nature* **446**, 782-786 (2007).
7. Olaya-Castro, A., Lee, C. F., Fassioli Olsen, F.&Johnson, N. F. Efficiency of energy transfer in a light-harvesting system under quantum coherence. *Physical Review B* **78**(2008).
8. Caruso, F., Chin, A. W., Datta, A., Huelga, S. F.&Plenio, M. B. Highly efficient energy excitation transfer in light-harvesting complexes: The fundamental role of noise-assisted transport. *Journal of Chemical Physics* **131**(2009).
9. Rebentrost, P., Mohseni, M., Kassal, I., Lloyd, S.&Aspuru-Guzik, A. Environment-assisted quantum transport. *New Journal of Physics* **11**(2009).

10. Woller, J. G., Hannestad, J. K.&Albinsson, B. Self-assembled nanoscale DNA-porphyrin complex for artificial light harvesting. *J Am Chem Soc* **135**, 2759-2768 (2013).
11. Miller, R. A., Presley, A. D.&Francis, M. B. Self-assembling light-harvesting systems from synthetically modified tobacco mosaic virus coat proteins. *J Am Chem Soc* **129**, 3104-3109 (2007).
12. Ma, Y. Z., Miller, R. A., Fleming, G. R.&Francis, M. B. Energy transfer dynamics in light-harvesting assemblies templated by the tobacco mosaic virus coat protein. *Journal of Physical Chemistry B* **112**, 6887-6892 (2008).
13. Lee, Y. J. *et al.* Fabricating Genetically Engineered High-Power Lithium-Ion Batteries Using Multiple Virus Genes. *Science* **324**, 1051-1055 (2009).
14. Dang, X. N. *et al.* Virus-templated self-assembled single-walled carbon nanotubes for highly efficient electron collection in photovoltaic devices. *Nature Nanotechnology* **6**, 377-384 (2011).
15. Nam, Y. S. *et al.* Biologically templated photocatalytic nanostructures for sustained light-driven water oxidation. *Nature Nanotechnology* **5**, 340-344 (2010).
16. Ghosh, D. *et al.* M13-templated magnetic nanoparticles for targeted in vivo imaging of prostate cancer. *Nature Nanotechnology* **7**, 677-682 (2012).
17. Nam, Y. S. *et al.* Virus-Templated Assembly of Porphyrins into Light-Harvesting Nanoantennae. *Journal of the American Chemical Society* **132**, 1462-+ (2010).
18. Panitchayangkoon, G. *et al.* Long-lived quantum coherence in photosynthetic complexes at physiological temperature. *Proceedings of the National Academy of Sciences of the United States of America* **107**, 12766-12770 (2010).
19. Marvin, D. A., Welsh, L. C., Symmons, M. F., Scott, W. R. P.&Straus, S. K. Molecular structure of fd (f1, M13) filamentous bacteriophage refined with respect to X-ray fibre diffraction and solid-state NMR data supports specific models of phage assembly at the bacterial membrane. *Journal of Molecular Biology* **355**, 294-309 (2006).
20. Lankiewicz, L., Malicka, J.&Wiczk, W. Fluorescence resonance energy transfer in studies of inter-chromophoric distances in biomolecules. *Acta Biochimica Polonica* **44**, 477-489 (1997).
21. Turro, N. J., Ramamurthy, V.&Scaiano, J. C. *Modern molecular photochemistry of organic molecules*. (University Science Books, 2010).
22. Spence, M. T. Z.&Johnson, I. D. *The molecular probes handbook : a guide to fluorescent probes and labeling technologies*. 11th edn, (Live Technologies Corporation, 2010).
23. Noh, T. *et al.* Studies on aggregation of fluorescein derivatives by electroabsorption spectroscopy. *Molecular Crystals and Liquid Crystals Science and Technology Section a-Molecular Crystals and Liquid Crystals* **337**, 373-376 (1999).
24. Isom, D. G., Castaneda, C. A., Cannon, B. R.&Garcia-Moreno, B. Large shifts in pKa values of lysine residues buried inside a protein. *Proc Natl Acad Sci U S A* **108**, 5260-5265 (2011).

25. Marcelli, A., Foggi, P., Moroni, L., Gellini, C.&Salvi, P. R. Excited-state absorption and ultrafast relaxation dynamics of porphyrin, diprotonated porphyrin, and tetraoxaporphyrin dication. *J Phys Chem A* **112**, 1864-1872 (2008).
26. Haken, H.&Reineker, P. Coupled Coherent and Incoherent Motion of Excitons and Its Influence on Line Shape of Optical-Absorption. *Zeitschrift Fur Physik* **249**, 253-& (1972).
27. Haken, H.&Strobl, G. Exactly Solvable Model for Coherent and Incoherent Exciton Motion. *Zeitschrift Fur Physik* **262**, 135-148 (1973).

## Figure Legends

**Figure 1. Molecular models of the genetically engineered M13 viruses. The pVIII coat protein assemblies were reconstructed from the structural model (PDB number 2C0W). a**, A filamentous M13 virus is approximately 880 nm in length and ~ 7 nm in diameter and composed of 2,700 copies of the major coat protein pVIII, which provides a scaffold for excitation energy transport over chromophores in a light-harvesting antenna system. **b**,**c**, Zoomed-in M13 virus surfaces show the energy transfer networks between chromophore-binding sites for M13SF and M13CF, respectively (Blue color: N-terminus, orange: newly added lysine residue, and green: pre-existing lysine residue). Insets show schematic networks of energy transport in M13SF and M13CF, respectively. (Red gradient color of ellipse indicates exciton delocalization. Blue arrows show incoherent exciton hopping. For M13CF, pathways to any of the lysine binding sites are not shown because only 7% are occupied.) In the M13SF close inter-binding site distances of approximately 10 Å and 13 Å are formed among three pVIII proteins. M13CF has long inter-binding site distances of 28, 33 Å.

**Figure 2. Steady-state spectra and fluorescence quenching at room temperature. a,** Absorption and emission spectra of free donor (DN) and free acceptor. **b**, Fluorescence spectra of donor chromophores at excitation wavelength 495 nm. All samples have absorbance of 0.3 at 495 nm with 1 cm path-length of light. M13SF-DN indicates the virus with ~ 4,100 donors on the surface, and M13CF-DN indicates the virus with ~ 2,900 donors. Significant quenching is observed in M13SF-DN. The upper inset is a fluorescence microscope image of M13SF-DN (Excitation at 488 nm and detection at 528 nm). The bottom inset is a photograph taken under ambient light at the same absorbance of 0.5 with 1 mm path-length of light. The change in color is apparent between the two samples.

**Figure 3. Steady-state fluorescence data at room temperature showing exciton harvesting. a**, Total fluorescence energy upon donor excitation emitted from the acceptors as a function of acceptor concentration. A schematic representation of the experimental concept is shown in the inset for two possible donor-to-acceptor ratios. Black text denotes donor-to-acceptor ratios. **b**, Fluorescence energy normalized by the number of acceptors as a function of donor-to-acceptor ratio. Data normalized to have same maximum. Our fluorescence theory fits well to the M13CF and M13SF data. The donor-to-acceptor ratios are as follows: 16:1, 27:1, 72:1, 118:1, 236:1, 432:1, 627:1, and 734:1 for M13SF and 19:1, 43:1, 98:1, 159:1, 394:1 for M13CF.

**Figure 4. Transient-absorption (TA) spectra at room temperature. a**, Optical density change (ΔO.D.) map of donors assembled on the M13SF virus as a function of both delay time and wavelength. The sample was pumped at 470 nm. **b,** Normalized bleaching kinetics of optical density change (-ΔO.D.) probed at 500 nm as a function of delay time (dots). The bleaching traces were fitted by a triple-exponential function (solid lines).

**Figure 5. Comparison of classical and quantum transport theories for M13SF.** Numerical simulations on the normalized fluorescence data for M13SF. The classical walk description does not explain the M13SF. The newly developed Super-Förster theory and decohered quantum walk match the normalized fluorescence data of the M13SF.

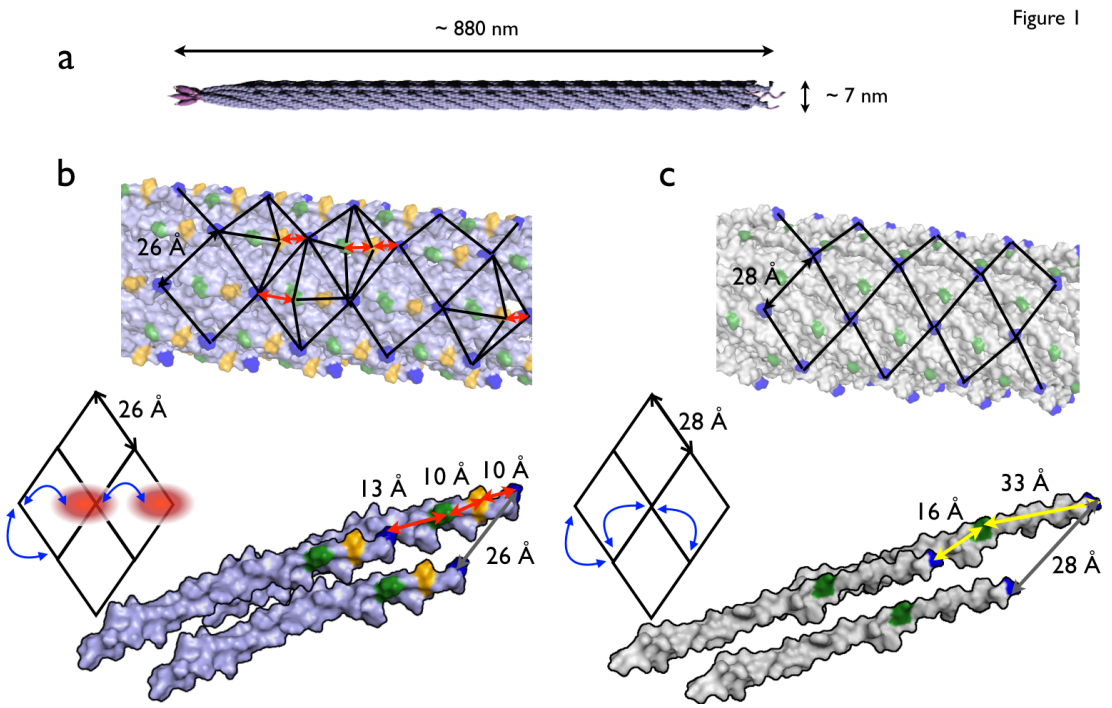

Figure 2

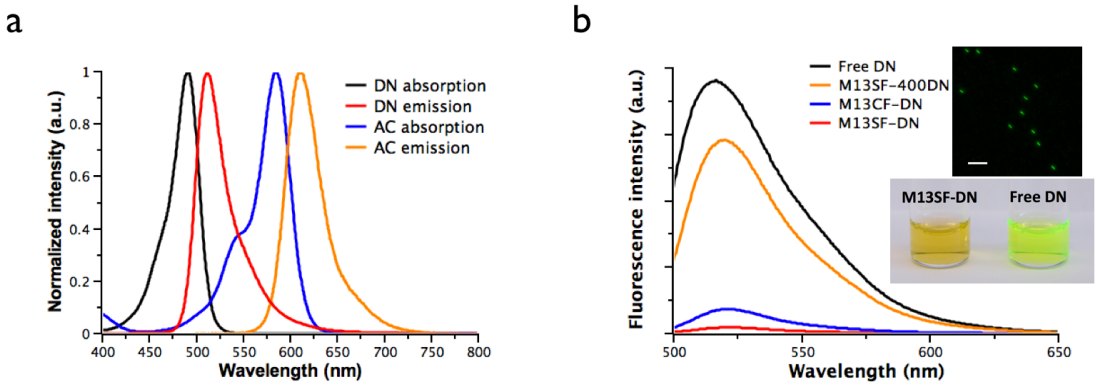


Figure 3

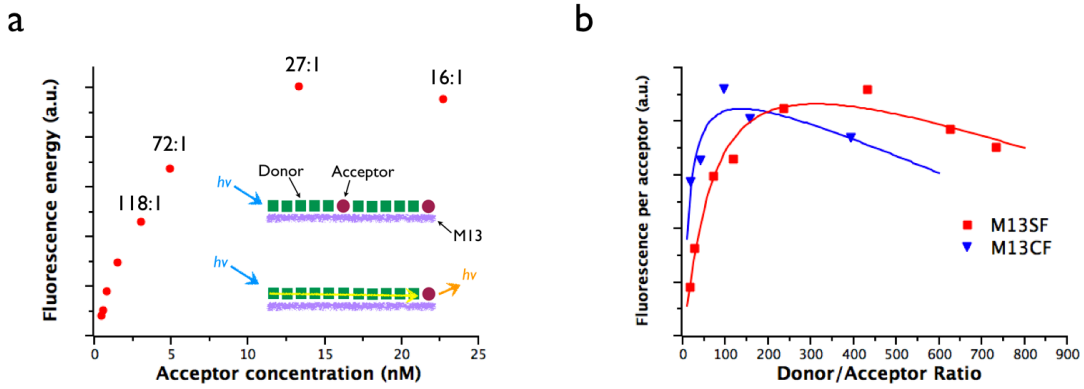

Figure 4

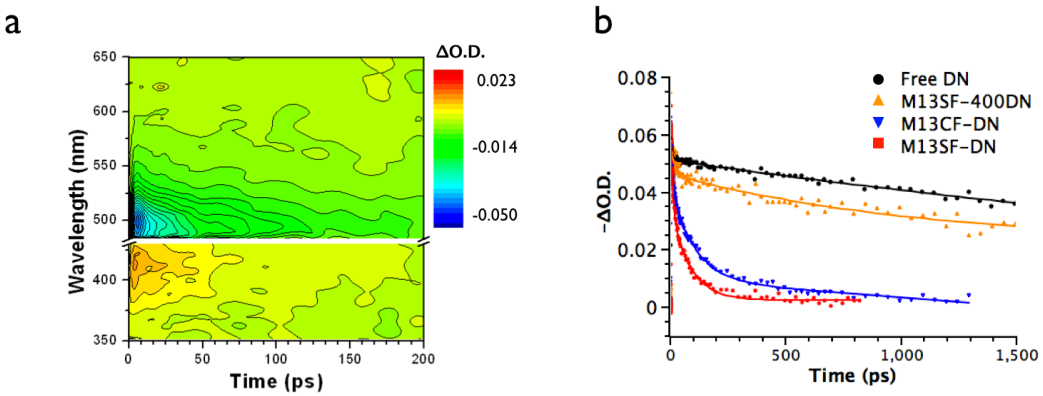


Figure 5